ADVANCED MATERIALS
www.advmat.de

# Direct Observation of Room-Temperature Magnetic Skyrmion Motion Driven by Ultra-Low Current Density in Van Der Waals Ferromagnets

*Yubin Ji, Seungmo Yang, Hyo-Bin Ahn, Kyoung-Woong Moon, Tae-Seong Ju, Mi-Young Im, Hee-Sung Han, Jisung Lee, Seung-young Park, Changgu Lee,* Kab-Jin Kim,* and Chanyong Hwang**

**The recent discovery of room-temperature ferromagnetism in 2D van der Waals (vdW) materials, such as $Fe_3GaTe_2$ (FGaT), has garnered significant interest in offering a robust platform for 2D spintronic applications. Various fundamental operations essential for the realization of 2D spintronics devices are experimentally confirmed using these materials at room temperature, such as current-induced magnetization switching or tunneling magnetoresistance. Nevertheless, the potential applications of magnetic skyrmions in FGaT systems at room temperature remain unexplored. In this work, the current-induced generation of magnetic skyrmions in FGaT flakes employing high-resolution magnetic transmission soft X-ray microscopy is introduced, supported by a feasible mechanism based on thermal effects. Furthermore, direct observation of the current-induced magnetic skyrmion motion at room temperature in FGaT flakes is presented with ultra-low threshold current density. This work highlights the potential of FGaT as a foundation for room-temperature-operating 2D skyrmion device applications.**

## 1. Introduction

2D van der Waals (vdW) materials have garnered significant interest as they offer an ideal platform for creating layered structures with a variety of properties, thereby enabling the exploration of low-dimensional physics.[1] These materials can be readily exfoliated and transferred to create heterostructure including Moiré patterns. The comparative advantage of using 2D ferromagnets is that layer imperfection can be avoided, which is quite critical in dealing with antiferromagnetic layers. In addition, even for ferromagnets, the uncertainties in the layer-dependent magnetization, critical temperature, and magnetic anisotropy will originate from this layer imperfection. Despite Mermin-Wagner theorem predicting the absence of spontaneous magnetism in 2D systems with isotropic Heisenberg models,[2] recent studies have revealed the possibility of long-range magnetic ordering in 2D systems, even in monolayers, by inducing strong uniaxial anisotropy.[3] A representative example of this layered ferromagnet, namely $Fe_3GeTe_2$, which exhibits ferromagnetism with a Curie temperature ($T_C$) of ≈200 K,[3a] has drawn a lot of attention for 2D spintronic applications;[3b,4] However, its low $T_C$ falling far below room

Y. Ji, K.-J. Kim
Department of Physics
Korea Advanced Institute of Science and Technology
Daejeon 34141, Republic of Korea
E-mail: kabjin@kaist.ac.kr

S. Yang, K.-W. Moon, T.-S. Ju, C. Hwang
Quantum Spin Team
Korea Research Institute of Standards and Science
Daejeon 34113, Republic of Korea
E-mail: cyhwang@kriss.re.kr

H.-B. Ahn
SKKU Advanced Institute of Nanotechnology
Sungkyunkwan University
Suwon 16419, Republic of Korea

M.-Y. Im, H.-S. Han
Center for X-ray Optics
Lawrence Berkeley National Laboratory
Berkeley, CA 94720, USA

H.-S. Han
Department of Materials Science and Engineering
Korea National University of Transportation
Chungju 27469, Republic of Korea

J. Lee, S.-young Park
Center for scientific instrumentation
Korea Basic Science Institute
Daejeon 34133, Republic of Korea

C. Lee
School of Mechanical Engineering
Sungykunkwan University
Suwon 16419, Republic of Korea
E-mail: peterlee@skku.edu

The ORCID identification number(s) for the author(s) of this article can be found under https://doi.org/10.1002/adma.202312013



**DOI: 10.1002/adma.202312013**

temperature hampers direct implementation in spintronic devices.[3a]

To overcome this challenge, researchers have explored $Fe_5GeTe_2$, which exhibits a higher $T_C$ of ≈300 K in bulk forms.[5] Nonetheless, the $T_C$ of its thin film structure still falls below room temperature, and the Fe-rich composition leads to complex magnetic orders,[6] requiring further development for practical spintronic applications. Doping $Fe_5GeTe_2$ with other 3d transition metals, such as cobalt or nickel, has been proposed as an alternative route to increase the $T_C$.[7] Despite their $T_C$ above room-temperature, there are several significant drawbacks that hinder utilization of them. First, the magnetic properties of these doped system can vary in the microscopic range. This can lead to unintentional local variation in doping concentrations,[7c] which can detrimentally affect the precise control of motion and generation of skyrmion. Second, in the case of Co-doped $Fe_5GeTe_2$, the magnetic properties of it exhibit a pronounced sensitivity to concentration and stacking order.[4k,7a,b] This has given rise to ongoing debates regarding the precise critical doping threshold at which the transition from ferromagnetic to antiferromagnetic phase occurs, posing further challenges for practical implementation.

Recently, $Fe_3GaTe_2$ (FGaT), where Ga replaces Ge in $Fe_3GeTe_2$, has emerged as a promising material, exhibiting $T_C$ between 350 and 380 K. Remarkably, even in a few nanometer-thick FGaT, it exhibits high saturation magnetization ($M_S$) and strong perpendicular magnetic anisotropy (PMA) at room temperature,[8] making it a compelling candidate for spintronic applications. Recent studies have experimentally demonstrated functional device operations at room temperature, such as magnetoresistance on spin-valve systems[9] and current-induced magnetization switching in FGaT;[10] However, an unexplored realm is the presence and dynamics behavior of topological magnetic textures within FGaT. Given the well-known defect-free nature of 2D systems, it becomes imperative to investigate the dynamics of these topological magnetic textures.

In this work, the generation of magnetic skyrmions through electrical current pulse injection under an external magnetic field is demonstrated, revealing that the skyrmion generation follows a thermal activation process. Moreover, current-driven magnetic skyrmion motion with an electrical pulse of the order of $10^9$ A/m$^2$ at room temperature was observed. Notably, the threshold current density for magnetic skyrmion motion in FGaT was two orders of magnitude smaller than that observed in similar 2D ferromagnetic materials such as $Fe_3GeTe_2$.[4h] Our findings highlight the potential of FGaT as a suitable material platform for 2D spintronic device applications.

## 2. Magnetic Properties of Single Crystal FGaT

**Figure 1a** illustrates the schematic representation of a layered structure of an FGaT 2D vdW system. As shown, an $Fe_3Ga$ slab (indicated by the red dashed box) is sandwiched between two Te atomic layers, and each FGaT layer is separated by a vdW gap.[8] In this layered structure, Fe atoms exhibit two valance states: $Fe^{3+}$ for the $Fe_I$ site and $Fe^{\circ}$ for the $Fe_{II}$ site,[8] whereas $Fe_3GeTe_2$ crystals possess $Fe^{2+}$ and $Fe^{3+}$ states. The presence of $Fe^0$ and high spin-polarized $Fe^{3+}$ states in the FGaT system may potentially give rise to ferromagnetism above room temperature.[8] To characterize the magnetic properties of an FGaT crystal grown by the self-flux method (see Experimental Section), temperature-dependent magnetization measurements on an FGaT crystal using a magnetic property measurement system (MPMS) was performed (Figure 1b). When a magnetic field is applied along the c-axis of the FGaT crystal, the magnetic moment increases as the temperature decreases. In contrast, under a magnetic field oriented within the a-b plane, the magnetic moment is significantly smaller compared with the c-axis case. This behavior can be attributed to the presence of PMA in the FGaT crystal, as the amplitude of the applied magnetic field (0.1 T) is insufficient to fully saturate the magnetic moment toward the applied field direction. The magnetic moments start to vanish from ≈360 K, indicating that the $T_C$ is above room temperature. To further elucidate the magnetic anisotropy features of the FGaT crystal, we measured magnetic hysteresis loops with a c-axis magnetic field (Figure 1c). The observed magnetic hysteresis loops along the c-axis do not display the typical square-shaped loop commonly associated with a uniaxial easy axis, and exhibit almost zero remanence magnetization ($M_r \equiv M(H = 0)/M_S$). Instead, these loops closely resemble the representative hard-axis loops; However, the tilted curve shape and the zero $M_r$ do not always indicate a hard axis. When a 2D ferromagnetic system with PMA, including a vdW system or a magnetic thin film, meets a particular ratio of material parameters, it can present a spontaneous stripe domain phase under a zero magnetic field.[11] Owing to the periodic alternation of domains representing two energy minimum states in a uniaxial PMA, $M_r$ becomes zero under a zero magnetic field. Consequently, the hysteresis loop shows a linear increase with an increase in the applied magnetic field by shrinking the width of the stripe domain, of which the magnetization direction is antiparallel to the magnetic field direction. The inset in Figure 1c displays the enlarged curves of the black dashed box region. All hysteresis loops show hysteresis behavior near the saturation point (Figure 1c, inset). This is a key signature indicating a spontaneous stripe domain phase, not a hard-axis magnetic hysteresis loop.[4k,12] This is because a stripe domain phase goes through a contraction when reaching the saturation state with an increasing magnetic field, whereas the nucleation process takes place with a decreasing magnetic field from the saturation state. Therefore, the hysteresis loops in Figure 1c demonstrate that the investigated FGaT crystals have a spontaneous stripe domain phase.

## 3. Magnetic Domain Structure in FGaT at Room Temperature

To examine the detailed magnetic domain structure of an FGaT flake, full-field magnetic transmission x-ray microscope (MTXM) at the Advanced Light Source (XM-1 BL 6.1.2) was utilized. For the MTXM experiment, the exfoliated FGaT flakes were carefully transferred onto a 200-nm-thick silicon nitride ($SiN_x$) membrane substrate using polycarbonate (PC) films and polydimethylsiloxane (PDMS). Then, gold electrodes were fabricated on the FGaT flake utilizing photolithography and lift-off techniques. The detailed information of sample fabrication can be found in the Methods section. **Figure 2a** represents the schematic of MTXM. Circularly polarized X-rays were employed to visualize the magnetic domains, in conjunction with an external magnetic field and electrical current injection. The intensity of the transmitted X-ray depends on the z-component of the magnetic moment of

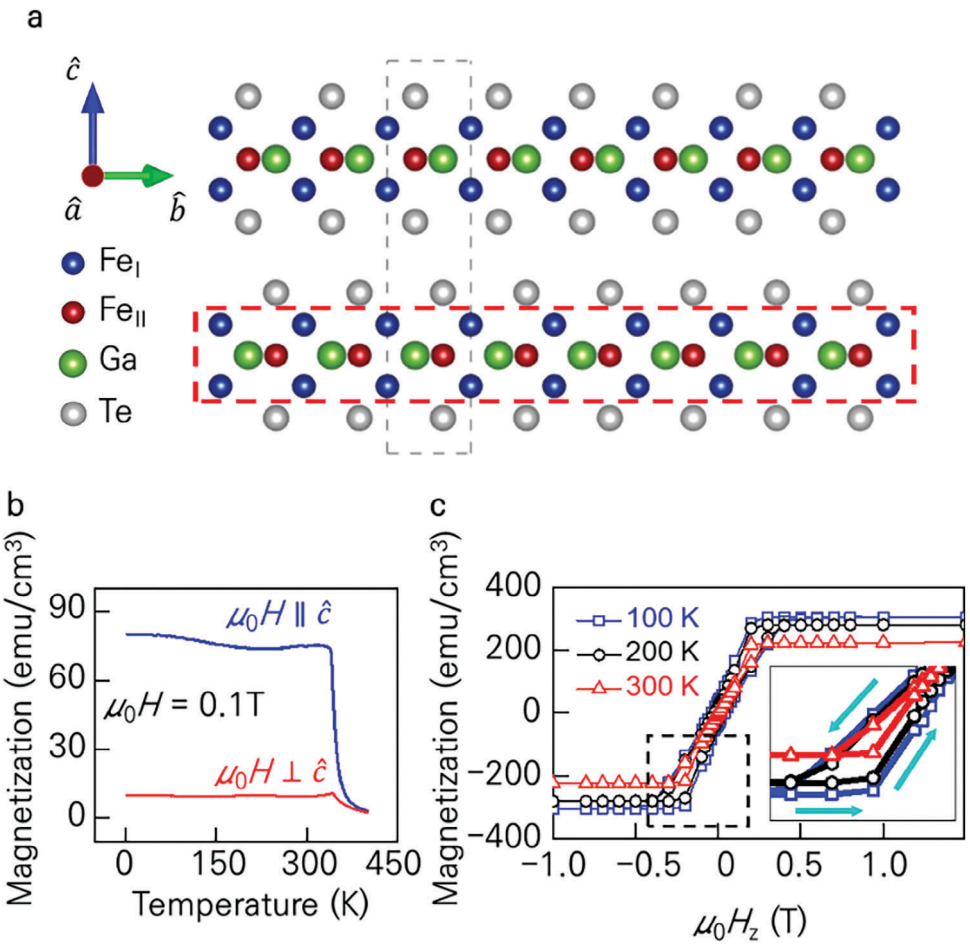


**Figure 1.** a) Schematic illustration of the layered crystal structure of FGaT. b) Temperature dependence of the magnetization in single crystal FGaT under a 0.1 T magnetic field. The red (blue) line represents the M-T curve for the magnetic field applied perpendicular to (along) the c-axis. c) External magnetic field response of magnetization in single crystal FGaT at various temperatures. The inset presents enlarged curves depicting the region marked by the black dashed box.

the FGaT flakes. Consequently, the magnetic domain structures can be imaged by the contrast differences between two magnetic domains (Figure 2a).

Our investigation commenced by examining the magnetic hysteresis loop along the c-axis for a 92.6-nm-thick FGaT flake using a polar magneto-optic Kerr effect (MOKE) microscope, as presented in Figure 2b. The discrepancy between hysteresis loop in Figure 1c of bulk crystal and that in Figure 2b of 92.6 nm thickness crystal is attributed to thickness-dependent dipolar interaction. This trend leads to a variation in the coercive field of FGaT depending on its thickness, which is similar to that of $Fe_3GeTe_2$.[13] Following a demagnetization process, the hysteresis loop starts from the zero value of the normalized MOKE intensity, as shown by the black curve in Figure 2b. As noted, the zero intensity under zero field indicates the stripe domain state, which can be confirmed by the corresponding magnetic domain image taken by the high-resolution full-field MTXM (Figure 2c). Here, bright and dark domains represent the $+z$ and $-z$ magnetic domains, respectively. Figure 2c–g presents the MTXM images captured at each magnetic field marked in Figure 2b, with increasing magnetic fields. The $-z$ stripe domains experience shrinking with increasing $+z$ magnetic fields because the $+z$ magnetic fields favor $+z$ magnetic domains due to Zeeman energy. The shrinking $-z$ stripe domains are eventually annihilated and become the $+z$ uniform state (Figure 2g). Then, starting from the $+z$ uniform state (Figure 2h), a sufficient $-z$ magnetic field nucleates $-z$ domains (Figure 2j), and then finally reaches the $-z$ uniform state (Figure 2l). During the above processes, magnetic skyrmions cannot be generated by applying magnetic fields. Furthermore, the stripe domain evolution behavior under the application of $z$-axis magnetic fields was investigated by varying the flake thickness from 91 to 172 nm. The findings revealed that within various thickness range, magnetic skyrmions cannot be created solely by applying magnetic fields (see Supporting Information 1).

## 4. Generation of Magnetic Skyrmion in FGaT by Thermal Activation at Room Temperature

In a perpendicularly magnetized thin-film, including a 2D vdW system, there exist three distinct ground states under specific perpendicular magnetic fields: the stripe domain state, the bubble domain (skyrmion) state, and the uniform state.[14] The transition

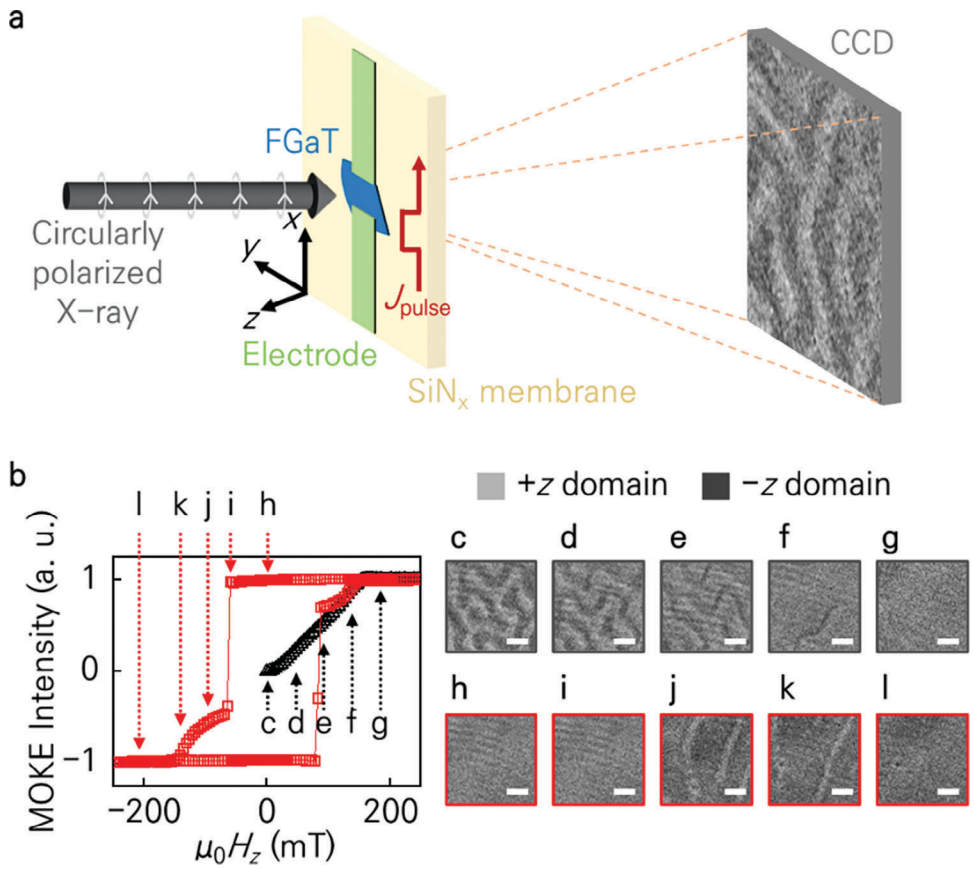


**Figure 2.** a) Schematic of MTXM. b) Magneto optical Kerr effect (MOKE) hysteresis loop while sweeping the magnetic field along the c-axis at room temperature. The black curve indicates the MOKE signal variation after demagnetization process. The polar MOKE microscope was utilized to examine the hysteresis loop. c–l) Corresponding room temperature MTXM magnetic domain images at each magnetic field marked in (b). The bright and dark regions correspond to the +z and -z direction of magnetic moment. The scale bars represent 500 nm.

between these states is feasible when overcoming energy barriers between the states, where thermal fluctuations play a crucial role in facilitating these transitions. It means that the applied magnetic fields do not cause sufficient perturbations to activate the transition from a stripe domain state to a bubble domain (skyrmion) state, therefore not leading to the generation of skyrmions. Hence, an additional external parameter is required to initiate skyrmion formation. To facilitate this process, we employ an electrical pulse injection scheme in conjunction with a particular external magnetic field. Here, applied electrical pulse increases the temperature of FGaT system and triggers thermal fluctuation which surpasses the energy barrier between two states. As shown in **Figure** 3a, we initiate with a stripe domain state under a zero magnetic field. Upon the application of an external magnetic field of +42.7 mT, the -z stripe domains contract (Figure 3b). Subsequently, the injection of an electrical pulse with a magnitude of $+2.66 \times 10^9$ A/m$^2$ for 100 µs results in the formation of a bunch of magnetic skyrmion bubbles (Figure 3c), where the type of these skyrmion bubble domains is anticipated to be the Néel capped skyrmion texture with the Bloch skyrmion in the middle. Detailed discussion related to the type of skyrmions can be found in Supporting Information 5. Excited skyrmion state persists even when the external magnetic field is removed. This is attributed to the aforementioned energy barrier between two states. This clearly demonstrates that the combined influence of magnetic fields and electrical currents induces a transition from the stripe domain state to the skyrmion bubble state.

We further investigate the influence of magnetic field strength and polarity on skyrmion generation. As illustrated in Figure 3e, skyrmions are also generated under a higher magnetic field of +83.1 mT, although the density of generated skyrmions is lower compared to the +42.7 mT magnetic field case (see Supporting Information 2 for a detailed information on the skyrmion density modulation). This suggests that there exists a sufficient range of magnetic field strengths capable of initiating magnetic skyrmion formation. Additionally, we find that a negative magnetic field of –83.1 mT produces skyrmions with opposite polarity (Figure 3g). Conversely, in the absence of a magnetic field, we observe no skyrmion generation, affirming that the current pulse alone cannot induce magnetic skyrmion formation. Hence, it becomes evident that both the magnetic field and electrical current are requisite for the generation of skyrmions.

To gain insight into the process of skyrmion generation, we conducted investigation on the dependence of skyrmion generation on the current pulse characteristics. **Figure** 4a presents a phase diagram illustrating skyrmion generation as a function of current pulse amplitude and duration. In this diagram, the red and blue regions correspond to the normalized skyrmion

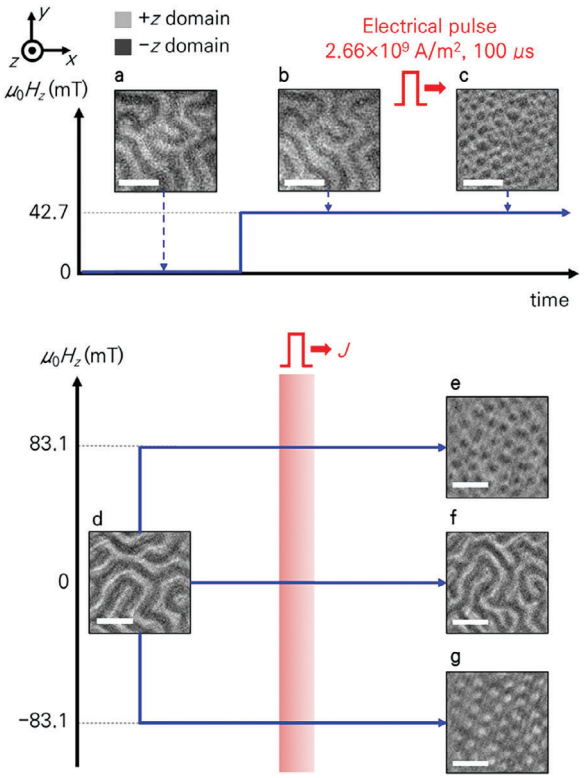


**Figure 3.** a–c) Skyrmion generation method utilizing electrical pulse under a magnetic field of 42.7 mT at room temperature. d–g) Magnetic skyrmion polarity control achieved by manipulating the direction of the external magnetic field. The pulse has an amplitude of 2.66 × $10^9$ A/$m^2$ and a width of 100 μs. The presence of a magnetic field is essential for magnetic skyrmion generation. All scale bars correspond to 1 μm.

number, $N_{sk}^{norm}$, being equal to 1 and 0, respectively. Here, $N_{sk}^{norm}$ is 0 when no skyrmions are present in the defined region and 1 when the region is fully occupied by skyrmions, as described in Figure 4b,d. A detailed explanation to determine $N_{sk}^{norm}$ can be found in the method section. As we increase the duration of current pulse, we observe a gradual transition from the stripe domain state to the skyrmion state, as illustrated by the MTXM images in Figure 4e–g. This suggests that the transition from the stripe state to the skyrmion state, achieved by overcoming the energy barrier, requires a finite amount of time.[15] We define this characteristic activation time as $\tau$, which corresponds to the time required for $N_{sk}^{norm} = 0.5$.

It is evident that the $\tau$ decreases as we increase the amplitude of the current pulse. To further elucidate the thermal activation process, we plot $\tau$ as a function of $J^2$ in Figure 4h. Within the framework of the Arrhenius law, $\tau$ can be related to the energy barrier as follows:

$$\tau = f^{-1} \exp\left(\frac{\Delta E_B}{k_B T}\right) = f^{-1} \exp\left(\frac{\Delta E_B}{k_B\left(T_0 + \alpha J^2\right)}\right) \quad (1)$$

Here, $f$ represents the attempted frequency, $\Delta E_B$ denotes the energy barrier between the stripe state and skyrmion state, $k_B$ is the Boltzmann constant, $T_0$ is the environmental temperature, and $T$ is the device temperature, which is modulated by

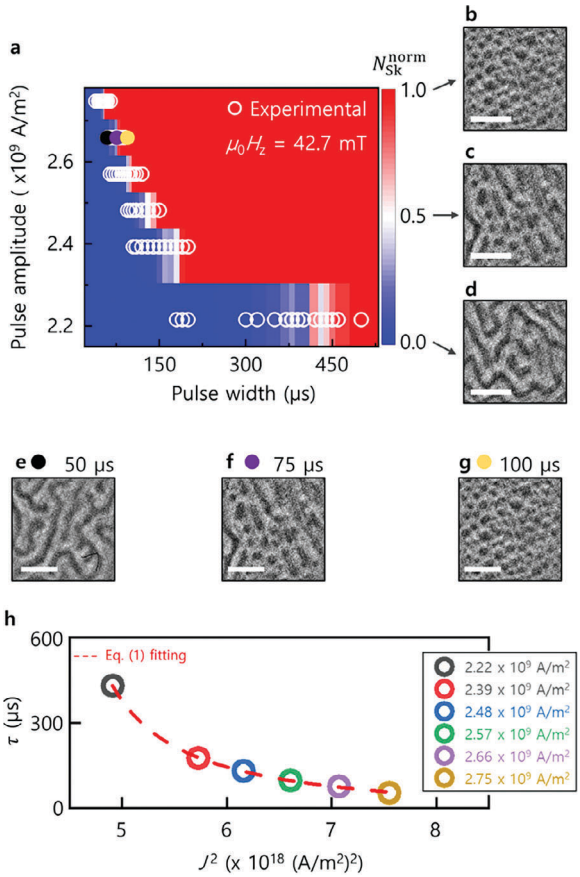


**Figure 4.** a) Phase diagram as a function of the electrical pulse amplitude and width for 172 nm-thick FGaT. The red ($N_{sk}^{norm} = 1$) and blue ($N_{sk}^{norm} = 0$) regions denote the skyrmion and stripe domain states, respectively. In the $0 < N_{sk}^{norm} < 1$ region, skyrmions and stripe domains coexist. The experimental measurements are represented by white circles. All experimental measurements were conducted at room temperature. b–d) MTXM images for each colored region. e,f) Pulse width dependent skyrmion generation condition with 2.66 × $10^9$ A/$m^2$ of amplitude. All scale bars correspond to 1 μm. g) The plot of $\tau$ with respect to $J^2$. The red dashed line corresponds to the fit according to equation (1).

$\alpha J^2$, with $\alpha$ representing the temperature coefficient. Notably, the experimental data closely conforms to the fitting line based on Equation (1), indicating that the skyrmion generation process is predominantly governed by the thermal activation process induced by current-induced Joule heating under the influence of the magnetic field. Our results on the thermal generation mechanism of skyrmions in FGaT are in good agreement with the previous reports.[4h,15,16]

## 5. Room Temperature Observation of Current-Induced Magnetic Skyrmion Motion in a FGaT

Having successfully demonstrated the generation of skyrmions in FGaT at room temperature, we now delve into our primary experiment: the observation of room temperature current-induced skyrmion motion. **Figure** 5a–e present MTXM images captured following the injection of a current pulse. First, magnetic

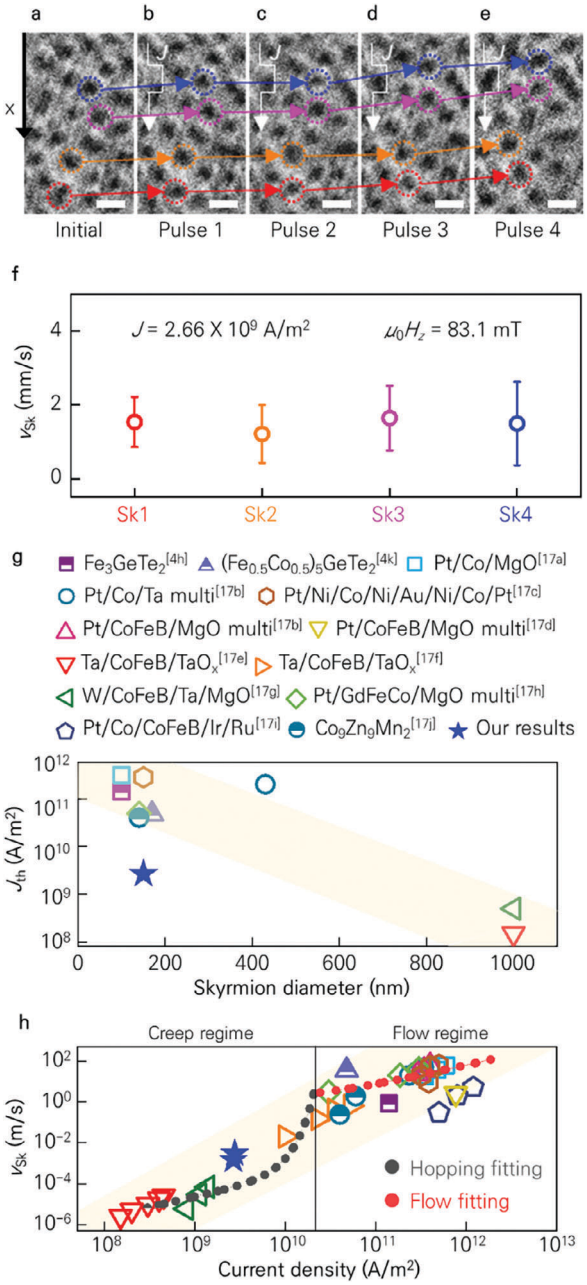


**Figure 5.** a–e) Direct imaging of current-induced skyrmion motion at room temperature using MTXM. The applied current pulse has an amplitude of 2.66 × $10^9$ A/$m^2$ and a width of 50 μs, under a magnetic field of 83.1 mT. The scale bars represent 300 nm. f,g) Plots illustrating the relationship between f) the threshold current density and skyrmion diameter and g) the skyrmion speed and current density for various magnetic systems.[4h,k,17]

skyrmions was generated by injecting an electrical current pulse of 2.66 × $10^9$ A/$m^2$ for 100 μs under the application of a perpendicular magnetic field of 83.1 mT, as presented in Figure 5a. Then, a relatively short electrical current pulse of 2.66 × $10^9$ A/$m^2$ for 50 μs was applied along the +*x*-axis, which is below the threshold required for skyrmion generation. Figure 5b shows a magnetic image taken after injecting the shorter current pulse. Consequently, these current pulses solely induce the motion of existing skyrmions without nucleating additional ones. Remarkably, the skyrmion responded to the electrical current pulse, as indicated by the guided path highlighted by colored circles in Figure 5a–e. It is noteworthy that the motion of magnetic skyrmions by current injection is parallel to the electron flow direction, indicating that spin-transfer torque drives the skyrmion motion.[18] One can realize the alignment of current density driving skyrmion motion and that required to form skyrmion phase, which is a simple coincidence. Explorations related to skyrmion dynamics and generation of skyrmion phase with higher current densities were hindered by the prevalence of thermal effect. Further research with the system that can effectively mitigate the thermal effect is needed to study the skyrmion dynamics with higher current densities and other current-induced effects associated with skyrmion formation.

Here, the current density used in this experiment is significantly lower than the previously values. To make a fair comparison with threshold current densities from prior studies,[4h,k,17] we plot the threshold current density as a function of skyrmion size, as the depinning drive force for skyrmion motion depends on its size.[19] As shown in Figure 5g, smaller skyrmions generally exhibit higher threshold currents; However, our results notably deviate from this trend. In FGaT systems, despite the relatively small size of skyrmions (≈150 nm), the required current densities do not exhibit a significant increase. This phenomenon can be attributed to the negligible effect of interfacial defect and lack of dangling bond in 2D system, which stems from the inherent vdW gaps and high crystallinity of it. This characteristic can significantly prevent the occurrence of surface roughness and intermixing in 2D system,[20] which are factors that determine the skyrmion dynamics. It is worth noting that FGaT demonstrates its superiority over other 2D magnets in terms of critical current for the skyrmion motion. The origin for significant reduction of critical current compared to $Fe_3GeTe_2$ is expected to be higher thermal energy resulting from the FGaT system's higher operation temperature, which aids in overcoming the depinning energy barrier. Additionally, the homogeneous crystal structure of FGaT can provide more well-ordered and clean circumstances compared to Co-doped $Fe_5GeTe_2$. This is relevant to aforementioned issue related to random doping-induced inhomogeneous magnetic defects in the introduction. Further simulation results for investigating the influence of defect sites on skyrmion motion can be found in Supporting Information 6. Consequently, our observations suggest that FGaT systems have the potential to serve as candidates for the development of 2D ferromagnet-based skyrmion devices operating at room temperature with low power consumption.

In addition, controlling the speed of skyrmions is also pivotal for their integration into spintronic applications. The speeds of the skyrmions, as marked in Figure 5a–e, are presented in Figure 5f, revealing an approximate speed of ≈1.5 mm $s^{-1}$. While this speed may appear relatively slow compared to previous studies, it is essential to consider that the driving current density employed here is considerably lower. Figure 5h illustrates the relationship between skyrmion speed and current density across various magnetic systems. Clearly, our data aligns with the trends observed in other studies. This suggests that skyrmion speeds can be significantly enhanced, reaching several meters per second,

with an increase in current density (more discussion in Supporting Information 4). Consequently, FGaT systems hold promise as candidates for the development of 2D ferromagnet-based skyrmion devices operating at room temperature and exhibiting low power consumption.

## 6. Conclusion

In summary, the magnetic skyrmion was observed in 2D ferromagnet FGaT at room temperature. The magnetic properties were examined by utilizing MPMS. MTXM was also adopted to image the magnetic domain structure and skyrmions. The field-dependent magnetic domain structure evolution was confirmed using both the MOKE microscope and MTXM. At room temperature, magnetic skyrmions were successfully generated by injecting an electrical pulse under an external magnetic field. The manipulation of the polarity and density of skyrmions was achieved by adjusting the external magnetic field. Through the adjustment of electrical pulses, the conditions for skyrmion generation were thoroughly investigated; We concluded that skyrmions are thermally generated, as revealed by the characteristic time scale analysis. Finally, current-induced skyrmion motion at room temperature was observed. The speeds of skyrmions in FGaT were measured to be a few mm/s under electrical pulse with the amplitudes of the order of $10^9$ A/m$^2$. It was found that the speed of skyrmions could be modulated by controlling the density of skyrmions and the electrical pulse amplitude. Because the observed phenomenon was achieved in a pristine FGaT system without further 3d metal doping, which can adversely affect the motion of skyrmions, FGaT may well be an attractive candidate for the future development of 2D vdW ferromagnet-based skyrmion devices and their application at room temperature.

## 7. Experimental Section

*Synthesis Method of Single Crystal FGaT*: FGaT crystal was synthesized by the self-flux method, in which Te takes a role of flux. A mixture of Fe powder, Ga lump, and Te pellets was prepared in a molar ratio of 1:1:2, and inserted into a quartz ampoule. The ampoule was purged with Ar gas several times, evacuated, and sealed. It was then placed in a box furnace and heated to 1273 K over 24 h and held at that temperature for an additional 24 h to form a homogeneous flux state of the inserted mixture. The sample was then cooled at a rate of 3 K/h until it reached 773 K and then cooled down to room temperature without further treatment.

*Sample Fabrication*: We first exfoliated FGaT flakes on a 300-nm-thick $SiO_x$ substrate using exfoliation tape. Conventional dry transfer method using polycarbonate (PC) film and polydimethylsiloxane (PDMS) was adopted to transfer FGaT flakes onto a 200-nm-thick $SiN_x$ membrane substrate from the 300-nm-thick $SiO_x$ substrate. The size of the FGaT flakes is ≈10 µm × 10 µm, with the thickness ranging from tens of nanometers to 180 nm. After transferring the FGaT flake from $SiO_x$ substrate to $SiN_x$ membrane substrate, we have employed the photolithography and lift-off techniques to fabricate the gold electrodes. We deposited a 2 nm of Ti layer for adhesion, followed by deposition of 100–200 nm of Au using sputtering system.

*Determination of the Normalized Generated Skyrmion Number ($N_{sk}^{norm}$)*: To determine $N_{sk}^{norm}$, we first count the number of isolated domains from the MTXM images. Next, domains attached to the edge of the image are excluded. Through this process, Figure 4g results in zero domains. The determined number of isolated domains is then normalized so that Figure 4e becomes 1.

## Supporting Information

Supporting Information is available from the Wiley Online Library or from the author.

## Acknowledgements

Y.J., S.Y., and H.-B.A. contributed equally to this work. This work was supported by the National Research Foundation of Korea (Grant Nos. NRF-2022M3H4A1A04071154, RS-2023-00207732, and RS-2023-00275259), and the Technology Innovation Program (or Industrial Strategic Technology Development Program) (20020286) funded by the Ministry of Trade, Industry & Energy (MOTIE, Korea), and works at the ALS were supported by U. S. Department of Energy (DE-AC02-05CH11231).

## Conflict of Interest

The authors declare no conflict of interest.

## Data Availability Statement

The data that support the findings of this study are available from the corresponding author upon reasonable request.

## Keywords

2D ferromagnets, skyrmion, spintronics

Received: November 12, 2023
Revised: January 5, 2024
Published online:

[1] a) A. F. Young, P. Kim, *Annu. Rev. Condens. Matter Phys.* **2011**, *2*, 101; b) A. Avsar, H. Ochoa, F. Guinea, B. Özyilmaz, B. J. van Wees, I. J. Vera-Marun, *Rev. Mod. Phys.* **2020**, *92*, 021003.
[2] N. D. Mermin, H. Wagner, *Phys. Rev. Lett.* **1966**, *17*, 1133.
[3] a) Z. Fei, B. Huang, P. Malinowski, W. Wang, T. Song, J. Sanchez, W. Yao, D. Xiao, X. Zhu, A. F. May, W. Wu, D. H. Cobden, J.-H. Chu, X. Xu, *Nat. Mater.* **2018**, *17*, 778; b) Y. Deng, Y. Yu, Y. Song, J. Zhang, N. Z. Wang, Z. Sun, Y. Yi, Y. Z. Wu, S. Wu, J. Zhu, J. Wang, X. H. Chen, Y. Zhang, *Nature* **2018**, *563*, 94; c) B. Huang, G. Clark, E. Navarro-Moratalla, D. R. Klein, R. Cheng, K. L. Seyler, D. Zhong, E. Schmidgall, M. A. McGuire, D. H. Cobden, W. Yao, D. Xiao, P. Jarillo-Herrero, X. Xu, *Nature* **2017**, *546*, 270; d) C. Gong, L. Li, Z. Li, H. Ji, A. Stern, Y. Xia, T. Cao, W. Bao, C. Wang, Y. Wang, Z. Q. Qiu, R. J. Cava, S. G. Louie, J. Xia, X. Zhang, *Nature* **2017**, *546*, 265; e) M. Bonilla, S. Kolekar, Y. Ma, H. C. Diaz, V. Kalappattil, R. Das, T. Eggers, H. R. Gutierrez, M.-H. Phan, M. Batzill, *Nat. Nanotechnol.* **2018**, *13*, 289.
[4] a) Ø. Johansen, V. Risinggård, A. Sudbø, J. Linder, A. Brataas, *Phys. Rev. Lett.* **2019**, *122*, 217203; b) K. Zhang, S. Han, Y. Lee, M. J. Coak, J. Kim, I. Hwang, S. Son, J. Shin, M. Lim, D. Jo, K. Kim, D. Kim, H.-W. Lee, J.-G. Park, *Adv. Mater.* **2021**, *33*, 2004110; c) K. Kim, J. Seo, E. Lee, K. T. Ko, B. S. Kim, B. G. Jang, J. M. Ok, J. Lee, Y. J. Jo, W. Kang, J. H. Shim, C. Kim, H. W. Yeom, B. Il Min, B.-J. Yang, J. S. Kim, *Nat. Mater.* **2018**, *17*, 794; d) X. Wang, J. Tang, X. Xia, C. He, J. Zhang, Y. Liu, C. Wan, C. Fang, C. Guo, W. Yang, Y. Guang, X. Zhang, H. Xu, J. Wei, M. Liao, X. Lu, J. Feng, X. Li, Y. Peng, H. Wei, R. Yang, D. Shi, X. Zhang, Z. Han, Z. Zhang, G. Zhang, G. Yu, X. Han, *Sci. Adv.* **2019**, *5*, eaaw8904; e) I. Shin, W. J. Cho, E.-S. An, S. Park, H.-W. Jeong, S. Jang, W. J. Baek,

S. Y. Park, D.-H. Yang, J. H. Seo, G.-Y. Kim, M. N. Ali, S.-Y. Choi, H.-W. Lee, J. S. Kim, S. D. Kim, G.-H. Lee, *Adv. Mater.* **2022**, *34*, 2101730; f) I. H. Kao, R. Muzzio, H. Zhang, M. Zhu, J. Gobbo, S. Yuan, D. Weber, R. Rao, J. Li, J. H. Edgar, J. E. Goldberger, J. Yan, D. G. Mandrus, J. Hwang, R. Cheng, J. Katoch, S. Singh, *Nat. Mater.* **2022**, *21*, 1029; g) Y. Wu, S. Zhang, J. Zhang, W. Wang, Y. L. Zhu, J. Hu, G. Yin, K. Wong, C. Fang, C. Wan, X. Han, Q. Shao, T. Taniguchi, K. Watanabe, J. Zang, Z. Mao, X. Zhang, K. L. Wang, *Nat. Commun.* **2020**, *11*, 3860; h) T.-E. Park, L. Peng, J. Liang, A. Hallal, F. S. Yasin, X. Zhang, K. M. Song, S. J. Kim, K. Kim, M. Weigand, G. Schütz, S. Finizio, J. Raabe, K. Garcia, J. Xia, Y. Zhou, M. Ezawa, X. Liu, J. Chang, H. C. Koo, Y. D. Kim, M. Chshiev, A. Fert, H. Yang, X. Yu, S. Woo, *Phys. Rev. B* **2021**, *103*, 104410; i) B. Ding, Z. Li, G. Xu, H. Li, Z. Hou, E. Liu, X. Xi, F. Xu, Y. Yao, W. Wang, *Nano Lett.* **2020**, *20*, 868; j) M. Yang, Q. Li, R. V. Chopdekar, R. Dhall, J. Turner, J. D. Carlström, C. Ophus, C. Klewe, P. Shafer, A. T. N'Diaye, J. W. Choi, G. Chen, Y. Z. Wu, C. Hwang, F. Wang, Z. Q. Qiu, *Sci. Adv.* **2020**, *6*, eabb5157; k) H. Zhang, D. Raftrey, Y.-T. Chan, Y.-T. Shao, R. Chen, X. Chen, X. Huang, J. T. Reichanadter, K. Dong, S. Susarla, L. Caretta, Z. Chen, J. Yao, P. Fischer, J. B. Neaton, W. Wu, D. A. Muller, R. J. Birgeneau, R. Ramesh, *Sci. Adv.* **2022**, *8*, eabm7103; l) Z. Wang, D. Sapkota, T. Taniguchi, K. Watanabe, D. Mandrus, A. F. Morpurgo, *Nano Lett.* **2018**, *18*, 4303; m) H. Lin, F. Yan, C. Hu, Q. Lv, W. Zhu, Z. Wang, Z. Wei, K. Chang, K. Wang, *ACS Appl. Mater. Interfaces* **2020**, *12*, 43921; n) S. Albarakati, C. Tan, Z.-J. Chen, J. G. Partridge, G. Zheng, L. Farrar, E. L. H. Mayes, M. R. Field, C. Lee, Y. Wang, Y. Xiong, M. Tian, F. Xiang, A. R. Hamilton, O. A. Tretiakov, D. Culcer, Y.-J. Zhao, L. Wang, *Sci. Adv.* **2019**, *5*, eaaw0409.

[5] A. F. May, D. Ovchinnikov, Q. Zheng, R. Hermann, S. Calder, B. Huang, Z. Fei, Y. Liu, X. Xu, M. A. McGuire, *ACS Nano* **2019**, *13*, 4436.

[6] M. Tang, J. Huang, F. Qin, K. Zhai, T. Ideue, Z. Li, F. Meng, A. Nie, L. Wu, X. Bi, C. Zhang, L. Zhou, P. Chen, C. Qiu, P. Tang, H. Zhang, X. Wan, L. Wang, Z. Liu, Y. Tian, Y. Iwasa, H. Yuan, *Nat. Electron.* **2023**, *6*, 109.

[7] a) A. F. May, M.-H. Du, V. R. Cooper, M. A. McGuire, *Phys. Rev. Mater.* **2020**, *4*, 074008; b) C. Tian, F. Pan, S. Xu, K. Ai, T. Xia, P. Cheng, *Appl. Phys. Lett.* **2020**, *116*, 202402; c) X. Chen, Y.-T. Shao, R. Chen, S. Susarla, T. Hogan, Y. He, H. Zhang, S. Wang, J. Yao, P. Ercius, D. A. Muller, R. Ramesh, R. J. Birgeneau, *Phys. Rev. Lett.* **2022**, *128*, 217203.

[8] G. Zhang, F. Guo, H. Wu, X. Wen, L. Yang, W. Jin, W. Zhang, H. Chang, *Nat. Commun.* **2022**, *13*, 5067.

[9] a) W. Jin, G. Zhang, H. Wu, L. Yang, W. Zhang, H. Chang, *ACS Appl. Mater. Interfaces* **2023**, *15*, 36519; b) W. Jin, G. Zhang, H. Wu, L. Yang, W. Zhang, H. Chang, *Nanoscale* **2023**, *15*, 5371; c) H. Yin, P. Zhang, W. Jin, B. Di, H. Wu, G. Zhang, W. Zhang, H. Chang, *CrystEngComm* **2023**, *25*, 1339; d) H. Pan, C. Zhang, J. Shi, X. Hu, N. Wang, L. An, R. Duan, P. Deb, Z. Liu, W. Gao, *ACS Mater. Lett.* **2023**, *5*, 2226.

[10] W. Li, W. Zhu, G. Zhang, H. Wu, S. Zhu, R. Li, E. Zhang, X. Zhang, Y. Deng, J. Zhang, L. Zhao, H. Chang, K. Wang, *Adv. Mater.* **2023**, *35*, 2303688.

[11] T. N. G. Meier, M. Kronseder, C. H. Back, *Phys. Rev. B* **2017**, *96*, 144408.

[12] L. Belliard, J. Miltat, V. Kottler, V. Mathet, C. Chappert, T. Valet, *J. Appl. Phys.* **1997**, *81*, 5315.

[13] C. Tan, J. Lee, S. G. Jung, T. Park, S. Albarakati, J. Partridge, M. R. Field, D. G. McCulloch, L. Wang, C. Lee, *Nat. Commun.* **2018**, *9*, 1554.

[14] N. Saratz, U. Ramsperger, A. Vindigni, D. Pescia, *Phys. Rev. B* **2010**, *82*, 184416.

[15] I. Lemesh, K. Litzius, M. Böttcher, P. Bassirian, N. Kerber, D. Heinze, J. Zázvorka, F. Büttner, L. Caretta, M. Mann, M. Weigand, S. Finizio, J. Raabe, M. Y. Im, H. Stoll, G. Schütz, B. Dupé, M. Kläui, G. S. D. Beach, *Adv. Mater.* **2018**, *30*, 1805461.

[16] a) W. Legrand, D. Maccariello, N. Reyren, K. Garcia, C. Moutafis, C. Moreau-Luchaire, S. Collin, K. Bouzehouane, V. Cros, A. Fert, *Nano Lett.* **2017**, *17*, 2703; b) S. G. Je, D. Thian, X. Chen, L. Huang, D. H. Jung, W. Chao, K. S. Lee, J. I. Hong, A. Soumyanarayanan, M. Y. Im, *Nano Lett.* **2021**, *21*, 1253; c) Z. Wang, M. Guo, H.-A. Zhou, L. Zhao, T. Xu, R. Tomasello, H. Bai, Y. Dong, S.-G. Je, W. Chao, H.-S. Han, S. Lee, K.-S. Lee, Y. Yao, W. Han, C. Song, H. Wu, M. Carpentieri, G. Finocchio, M.-Y. Im, S.-Z. Lin, W. Jiang, *Nat. Electron.* **2020**, *3*, 672.

[17] a) R. Juge, S.-G. Je, D. d. S. Chaves, L. D. Buda-Prejbeanu, J. Peña-Garcia, J. Nath, I. M. Miron, K. G. Rana, L. Aballe, M. Foerster, F. Genuzio, T. O. Mentes, A. Locatelli, F. Maccherozzi, S. S. Dhesi, M. Belmeguenai, Y. Roussigné, S. Auffret, S. Pizzini, G. Gaudin, J. Vogel, O. Boulle, *Phys. Rev. Appl.* **2019**, *12*, 044007; b) S. Woo, K. Litzius, B. Krüger, M.-Y. Im, L. Caretta, K. Richter, M. Mann, A. Krone, R. M. Reeve, M. Weigand, P. Agrawal, I. Lemesh, M.-A. Mawass, P. Fischer, M. Kläui, G. S. D. Beach, *Nat. Mater.* **2016**, *15*, 501; c) A. Hrabec, J. Sampaio, M. Belmeguenai, I. Gross, R. Weil, S. M. Chérif, A. Stashkevich, V. Jacques, A. Thiaville, S. Rohart, *Nat. Commun.* **2017**, *8*, 15765; d) L.-M. Kern, B. Pfau, V. Deinhart, M. Schneider, C. Klose, K. Gerlinger, S. Wittrock, D. Engel, I. Will, C. M. Günther, R. Liefferink, J. H. Mentink, S. Wintz, M. Weigand, M.-J. Huang, R. Battistelli, D. Metternich, F. Büttner, K. Höflich, S. Eisebitt, *Nano Lett.* **2022**, *22*, 4028; e) W. Jiang, P. Upadhyaya, W. Zhang, G. Yu, M. B. Jungfleisch, F. Y. Fradin, J. E. Pearson, Y. Tserkovnyak, K. L. Wang, O. Heinonen, S. G. E. t. Velthuis, A. Hoffmann, *Science* **2015**, *349*, 283; f) W. Jiang, X. Zhang, G. Yu, W. Zhang, X. Wang, M. Benjamin Jungfleisch, John E. Pearson, X. Cheng, O. Heinonen, K. L. Wang, Y. Zhou, A. Hoffmann, Suzanne G. E. te Velthuis, *Nat. Phys.* **2017**, *13*, 162; g) M. Song, M. You, S. Yang, T.-S. Ju, K.-W. Moon, C. Hwang, K.-W. Kim, A. M. G. Park, K.-J. Kim, *Adv. Mater.* **2022**, *34*, 2203275; h) S. Woo, K. M. Song, X. Zhang, Y. Zhou, M. Ezawa, X. Liu, S. Finizio, J. Raabe, N. J. Lee, S.-I. Kim, S.-Y. Park, Y. Kim, J.-Y. Kim, D. Lee, O. Lee, J. W. Choi, B.-C. Min, H. C. Koo, J. Chang, *Nat. Commun.* **2018**, *9*, 959; i) T. Dohi, S. DuttaGupta, S. Fukami, H. Ohno, *Nat. Commun.* **2019**, *10*, 5153; j) L. Peng, K. Karube, Y. Taguchi, N. Nagaosa, Y. Tokura, X. Yu, *Nat. Commun.* **2021**, *12*, 6797.

[18] D. C. Ralph, M. D. Stiles, *J. Magn. Magn. Mater.* **2008**, *320*, 1190.

[19] a) L. Berges, E. Haltz, S. Panigrahy, S. Mallick, R. Weil, S. Rohart, A. Mougin, J. Sampaio, *Phys. Rev. B* **2022**, *106*, 144408; b) A. Salimath, A. Abbout, A. Brataas, A. Manchon, *Phys. Rev. B* **2019**, *99*, 104416.

[20] X. Zhang, Y. Zhang, H. Yu, H. Zhao, Z. Cao, Z. Zhang, Y. Zhang, *Adv. Mater.* **2022**, *35*, 2207966.